On the effects of non-Gaussian wavepackets on double slit interference patterns

Shaarav Ayachit

1) *Introduction*

A wavepacket is defined as a superposition of plane waves with finite spectral width and spatial localisation arising from Fourier structure [1]. For harmonic waves with different momenta, the following function is used to express the wavepacket:

$$\Psi(x) = \frac{1}{\sqrt{2\pi\hbar}} \int_{-\infty}^{+\infty} \phi(p) e^{ipx/\hbar} \quad \textbf{(1)}$$

Where $\phi(p)$ is the momentum space envelope function. This equation determines the range and weight of momentum values, i.e. Δp .

These wavepackets can be constructed through addition of a large number of waves, which interfere destructively everywhere except a small region, which in turn localises the wave to that region. This constriction of location is due to Heisenberg's uncertainty principle, which mathematically shows that the variance in momenta and the variance in position are inversely constrained [2]. This is expressed as:

$$\Delta x \cdot \Delta p \geq \frac{\hbar}{2} \quad \textbf{(2)}$$

Where p is momentum and x is position.

The time evolution of such a packet is determined by the Schrödinger equation: each plane-wave component evolves with a phase factor $e^{-i\omega(k)t}$ depending on its frequency $\omega(k)$.

Because the different momentum components acquire different phase shifts, the shape of the wave packet in position space changes in time. The group velocity $v_g = d\omega/dk$ determines the motion of the packet's peak, while the second derivative of $\omega(k)$with respect to k governs how much the packet spreads or disperses. Mathematically, this is shown as:

$$v_g = \frac{d\omega}{dk}, \frac{d^2\omega}{dk^2} \neq 0 . \quad \textbf{(3)}$$

For a free particle with a quadratic dispersion relation, the characteristic width, $\sigma(t)$, of an initially localized wave packet grows with time due to dispersion. The degree and rate of spreading depend on the initial momentum spread and the higher-order derivatives of the dispersion relation [3].

We therefore argue that in a double-slit experiment (DSE) setup, this evolution matters because the interference pattern observed on the detection screen depends on how the waves superimpose and interfere after passing through the slits. A packet that spreads more rapidly will have a broader spatial extent when reaching the slits, affecting the final pattern's intensity, (both maximum and minimum) visibility and even its fringe count.

Different functional forms of the initial wave packet (e.g., Gaussian vs. Lorentzian) have different momentum distributions and therefore different dispersion behaviors [4]. Thus, this should lead to distinct interference outcomes: packets with heavier tails or larger spectral variance will spread differently—and hence interfere differently—than those with narrow, smooth momentum profiles.

Despite this, Lorentzian wavepackets are less commonly used in non-relativistic quantum mechanics, stemming from the assumption that it is a fully Galilean invariant theory [5]. Gaussian wavepackets are, thus, preferred because they allow closed-form solutions under the Fourier transformation, which simplifies the prediction of interference effects [6-10].

Hence, this study quantitatively and qualitatively compares Gaussian and non-Gaussian packets to assess their influence on interference patterns, thereby evaluating the adequacy of standard Gaussian assumptions.

(2) Theoretical background

As seen previously, the model for the waves used in this study was as following:

$$\Psi(x) = Acos(kx) \cdot Envelope(x) \quad \textbf{(4)}$$

where k is the wave number, and $cos(kx)$ represents the carrier wave**,** which is a periodic component describing oscillation. The function $Envelope(x)$ modulates the amplitude, defining the spatial localisation of the wave packet (e.g., Gaussian or Lorentzian form). Note that this is a model ansatz, only working as a heuristic for modelling the wave. The exact definition is examined later in the 'Methodology' section.

While $cos(kx)$ is used here for illustrative simplicity, other sinusoidal functions can equivalently serve as carrier waves in the construction of wave packets, depending on boundary conditions and the problem setup.

Though $\Psi(x)$ (in quantum mechanics) is generally complex, the model uses a real-valued wave function. The study only observes effects on intensity and fringe count, which are independent of relative phase effects, justifying the use of a real-valued wavefunction. For particles confined to a region (e.g., an electron in a box, atomic orbitals), the solutions to the Schrödinger equation can naturally yield real wavefunctions, such as those described by Hermite polynomials for the quantum harmonic oscillator [11].

Additionally, another crucial mathematical operation was normalising the Lorentzian and Gaussian wavepackets before making subsequent comparisons between the results obtained.

Normalisation is a basic requirement in quantum mechanics, ensuring that the wavefunction maintains a consistent probabilistic interpretation [12] **.** By normalising a function, we ensure that the sum of all possibilities is 1. Unlike Gaussian, a Lorentzian wave packet can have extremely large peaks (with $I_{max} = 115\ arbitrary\ units$ when a Gaussian wave packet enforced under the same conditions would yield a peak of less than 1). This makes it harder to objectively compare the square modulus of a wavefunction, $|\Psi(x)|^2$, which represents the probability density of finding a particle at position x. For this interpretation to not lose its probabilistic meaning, the total probability of finding the particle somewhere in space must be exactly 1. This is enforced by the normalisation condition [13]:

$$\int_{-\infty}^{+\infty} |\Psi(x)|^2 dx = 1 \quad \textbf{(5)}$$

Furthermore, in interference-based studies like the DSE, failing to normalise the wave packet introduces inconsistencies, as any observed differences in intensity or visibility could stem from differing overall amplitudes[1] rather than pure physical behaviour of the packet's shape.

This is particularly relevant when comparing different wave packets. Gaussian wave packets decay rapidly due to their short tail, concentrating the probability density near the centre, whereas Lorentzian packets decay more slowly. This property causes the Lorentzian wave packet to have large localised peaks of probability distributions (rather than the traditional Gaussian probability distribution) as is shown by the graph below. This spikes the peak intensity to extremely large values.

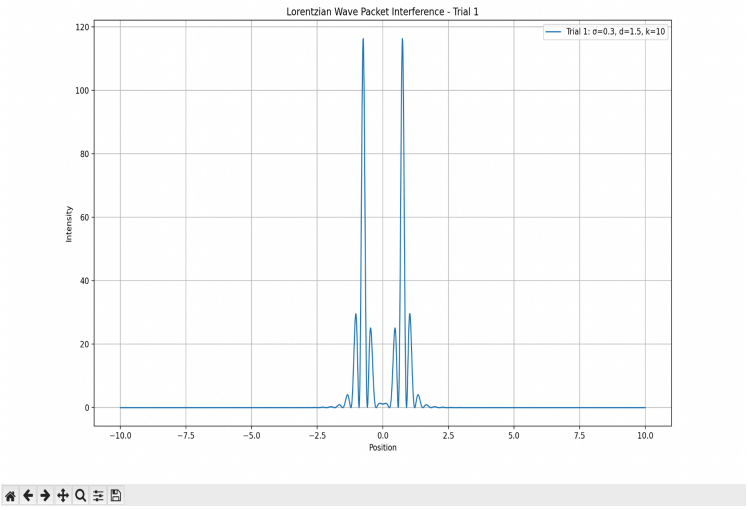

Figure 2.1: graph of intensity vs. position when the wavefunction is not normalised.

Moreover, two key 'observable' traits were used to compare interference patterns throughout the study. These were fringe count and peak intensity (I_{max}).

Fringe count is not a fundamental quantum observable, but rather an experimental value whose definition may vary per experiment [14]. For the purpose of the setup in the study, the fringe count is defined as the number of bright fringes [15], identified as local maxima in the normalised intensity profile $|\Psi(x)|^2$. To calculate the fringe count, the number of peaks on the graph of normalised intensity (y-axis) versus position (x-axis) was counted. Fringe count is dependent on geometrical features like the wavelength, the distance to the screen, the slit separation [16], and also the coherence length, which is affected by the choice of wavepacket

[1] Demonstrated by figure 2.1. While this result is physically still meaningful, it is the concept of Born's rule to ensure that the function is correct probabilistically; ensuring the sum of all probabilities remains 1.

[17]. Thus, by keeping geometrical features constant, we examined the effect of wavepackets on fringe count.

Peak intensity (I_{max}) refers to the maximum brightness or amplitude of the interference pattern at the screen, typically corresponding to the central fringe. This trait is particularly important because it reflects the constructive overlap of wave amplitudes and indicates how much of the particle's probability density contributes to the most likely detection location. If the wave packet has long tails, such as in the Lorentzian case [18], the amplitude at the centre may be less sharply defined than for a Gaussian, which concentrates its probability density near the centre due to rapid decay. Thus, peak intensity is useful for assessing how concentrated or diluted the particle's probability is in space, depending on the wave packet used. Peak intensity was simply calculated by measuring the global maximum value on the plot of normalised intensity against position.

The study also considered using visibility as a metric used with standard interference analyses. It quantifies the contrast between the bright and dark fringes and serves as a direct indicator of coherence between the interfering waves and how "wave-like" the interference behaviour is. Visibility can be calculated using the following equation:

$$V = \frac{I_{max} - I_{min}}{I_{max} + I_{min}} \quad \textbf{(6)}$$

A perfectly coherent source yields maximum visibility ($V = 1$), while decoherence or mismatches in wave packet overlap reduce this value. In practice, when localised wave packets such as Lorentzian or Gaussian forms are used, complete cancellation may not occur at every point, thus, they will not be perfectly coherent. However, since the model of the study used coherent waves to simulate interference, it was not possible to compare visibilities (i.e., both had $V = 1$) [19].

Note that this study does not involve solving Schrödinger's equation, but rather, taking snapshots of spatial interference based on geometric or temporal changes to slit separation, width of the wavepackets and the wave number, rather than using the TDSE. This is a deliberate idealization used to purely analyse the effects statistically rather than dynamically.

(3) Methodology

3.1 Programming Environment

All experimental runs were conducted on a MacBook Pro (2019 model) using a 1.4 GHz Quad-Core Intel Core i5 processor and 8 GB 2133 MHz LPDDR3 memory.

Python 3.13.5 was used for all the runs, utilising the following external libraries: NumPy, Matplotlib, SciPy. All libraries' latest stable versions were used at the time of the study. NumPy was used for numerical arrays and operations, Matplotlib was used to plot the resultant graphs of intensity (y-axis) vs. position (x-axis) and SciPy was used to detect and display the number of peaks on the resultant graphs.

3.2 Condition Sets

To model variances in DSE setups, three critical [20] parameters were first chosen: the width of the wave packet[2], the separation of slits and the wave number of the modeled waves. These factors were chosen considering both ease of measurability and relevance to physical parameters of interference patterns. Then, 5 'condition sets' (i.e., groups containing defined values for the width of the wavepacket, the separation of slits and the wave number) were made, where each condition set had an assigned value of these 3 parameters. First Gaussian wave packets were used for conditions sets 1 through 5. This was then repeated with Lorentzian wave packets.

For the purpose of the code used, the width of the wave packet was expressed by γ, the separation of slits was expressed by d, and the wave number was expressed by k.

The following table summarises the values used for each condition set:

Condition set	γ	d	k

[2] For Gaussian packets, the width of the wavepacket corresponds to the spatial standard deviation, while for Lorentzian packets the width of the wavepacket is defined as the half-width at half-maximum. This physical difference arises from the nature of the wave packet itself, but it is ultimately the same measurement for both wavepackets.

1	0.7	1.3	14
2	0.8	2.3	16
3	0.9	3.3	18
4	1.0	4.3	20
5	1.1	5.3	22

T

Table 3.2.1 - values of each parameter in each condition set.

Note that the spatial domain was defined as $x = (-10, 10, 2000)$, without assigning a physical unit. Since numerical values were used purely for simulation, no real-world unit is imposed on any three of the parameters. Hence, all three spatial quantities have arbitrary spatial units.

3.3 Model

The model designed for the experiment followed a 6-step process to simulate the interference of two identical Lorentzian or Gaussian wave packets centered at positions +d/2 and -d/2.

The first step was to define the wave packet. For Lorentzian wave packets, it was done using the following function [21]:

$$\Psi_1(x) = \frac{cos(k(x-\frac{d}{2}))}{(x-\frac{d}{2})^2+\gamma^2} \quad \textbf{(7)}$$

For Gaussian wave packets, it was done using the following function [22]:

$$\Psi_1(x) = e^{\frac{(x-\frac{d}{2})^2}{2\gamma^2}} cos(k(x-\frac{d}{2})) \quad \textbf{(8)}$$

The following steps were the same for the model, regardless of whatever form of the wave packet was used.

Then, a second wave, psi2 would be modelled using the same function, only the position would be at -d/2 instead of +d/2.

The sum of these two waves,Ψ_{total}, was then computed by adding the two functions. This is represented by the following equation:

$$\Psi_{total} = \Psi_1(x) + \Psi_2(x) \quad \textbf{(9)}$$

Physically, this simulates the imposition of two waves being superpositioned to form interference patterns.

The second step was to normalise the wavefunction. A common pitfall when normalising wavefunctions in double-slit set ups is to individually normalise $\Psi_1(x)$ and $\Psi_2(x)$before adding those two functions together. This is incorrect as the superposition of two normalised packets does not necessarily remain normalised and the interference term (cross terms) introduces additional amplitude contributions, leading to an overestimation of total intensity, especially in overlapping regions [23].

To avoid this error, the model performed a global normalisation of the total intensity. This is done by first squaring the function psi_total, and then integrating it using the trapezoidal rule [24] to integrate the intensity over the domain x, effectively computing the area under the $|\Psi(x)|^2$ curve, using the equation below:

$$\int |\Psi(x)|^2 dx \approx trapz(|\Psi(x)|^2, x) \quad \textbf{(10)}$$

Note that the $|\Psi(x)|^2$ is interpreted as a probability density function reflected through changes in intensity at a particular position. The complex conjugate is not required as the wavefunction is real-valued.

The last step of normalisation is to divide each value in the intensity array by the total integral (norm_factor). This ensures that the area under the domain $x \in [-10, 10]$ is exactly 1.

The third step sets the spatial domain, x, by defining 2000 linearly spaced points between -10 and 10 using the NumPy function linspace.

The fourth step is to set the value of each parameter, γ, d and k, as per the condition set being tested.

The fifth step is a critical one, which is to dynamically model spatial coherence, by mimicking wave packet separation over time. This was done by modelling the original value of d as a function of time, t. The function was modelled in the following manner:

$$d(t) = d \cdot t \quad \textbf{(11)}$$

Where t is a parametric index (a factor of time) but not physical time itself.

Hence, as the time factor increases, the distance between slits increases, which means that there is less overlap between waves, which causes interference fringes to become narrower and increase in number, represented by an increased peak count.

This design mimics the temporal evolution seen in the Time-Dependent Schrödinger Equation (TDSE), where the wavefunction $\Psi(x, t + \delta t)$ is computed from $\Psi(x, t)$. Instead of evolving the wavefunction across discrete time steps using traditional TDSE solvers, this model simulates an analogous evolution by scanning a series of spatial configurations parameterised by a time-dependent separation function $d(t)$. By encoding temporal behavior into spatial parameter variation, this workaround offers a computationally efficient alternative to explore decoherence and temporal interference dynamics, without directly solving the full TDSE numerically.

The sixth and last step is to plot the graph of normalised intensity against position using the external library Matplotlib. The graph was also coded to include the peak intensity, the minimum intensity (points of global minima) and the peak count.

This process was repeated for every condition set, first using Gaussian wave packets, then using Lorentzian wave packets.

The diagram below summarises the six step model.

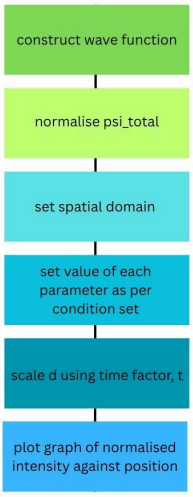

Figure 3.3.1 - six-step model to simulate double slit interference.

3.4 Assumptions

Certain assumptions were made by the model. These must be considered reproducing results from the same model. Thus, the following assumptions were made:

1) Wave packets were analysed in scalar fields as per the scalar diffraction theory that explicitly ignores polarization effects by treating the field as a scalar amplitude rather than a vector field. This is a standard approximation in optics when polarization does not significantly affect the intensity pattern being modeled [25].

2) The simulation analyses interference across a one-dimensional detector screen at a fixed distance from the slits. The screen acts as a line detector sampling intensity along one spatial axis.

3) Wave packets are assumed to travel in free space, with no potentials or medium effects, leading to an absence of external fields and other physical wave phenomena such as refraction. This assumption isolates the effects of interference.

(4) Results and Discussion

4.1 Time evolution with Gaussian wave packets

The first parameter to consider is how 'time-evolution' (as defined in the previous section) influenced the characteristics of the graphs. Four main plot characteristics were observed to compare how time evolution altered the resultant graph for Gaussian wave packets.

The first characteristic is the 'shape' of the graph. All graphs had one global maxima of intensity, like a traditional Gaussian curve, but then after a certain point of time (the value, t, of which fluctuated as per the condition set) in each condition set, the graph shifted into a shape with two global maxima. A representative case from condition set 1 is expressed below. Note that all graphs represent the scaled d value [d(t)] and not the original value of d as extrapolated from the condition sets.

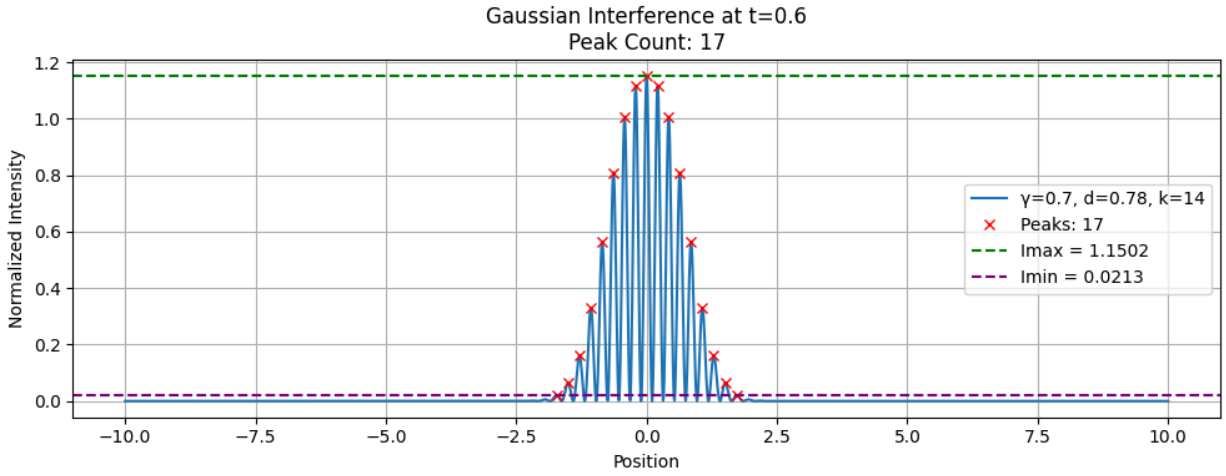

Figure 4.1.1 - Plot of Normalised intensity versus Position for condition set 1 at t=0.6. The graph shows one global maximum.

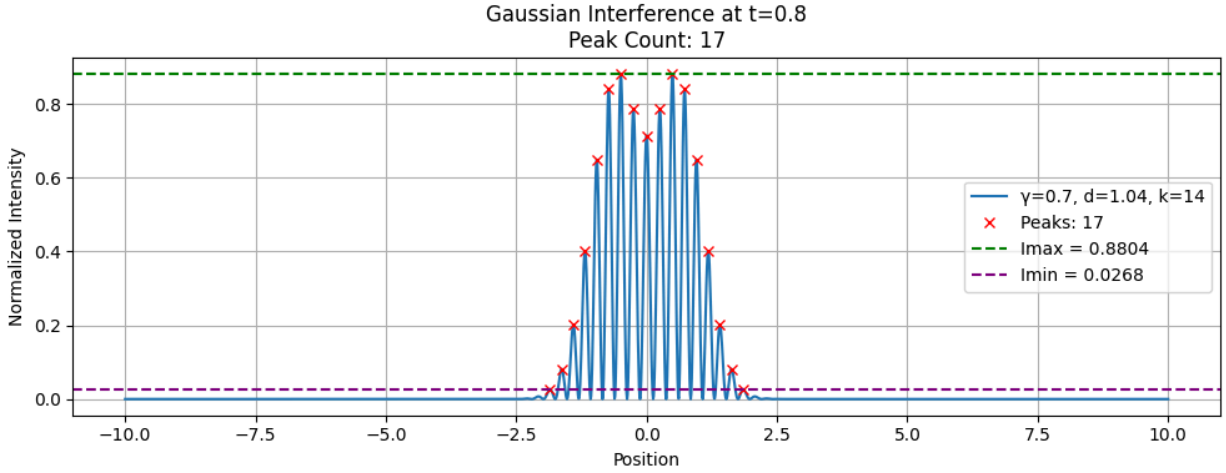

Figure 4.1.2 - Plot of Normalised intensity versus Position for condition set 1 at t=0.8. The graph shows two global maxima.

This phenomenon can be explained using the idea that waves are being separated as time evolves (i.e. dispersion of waves occurs) as distance between slits, d, increases over time as the function d(t) increases. A small value of d(t) leads to more overlap, so there are more constructive points of interference (than later) and leading to one global maxima (a central peak). As the wave function 'evolves' (or rather, is captured in a later time frame) d(t) increases so there is less superimposition of waves, causing individual 'lobes' to appear. This trend is expected to continue as time progresses.

However, the second characteristic, the time after which we observed this shift was not constant. In fact, a steady trend was observed as condition sets progressed from condition set 1 to condition set 5. This is to be expected as the constant 'd' increased, which contributed to the function d(t) increasing in value.

The table numerically expresses this trend, showing values of d and d(0.8) for Gaussian wavepackets. Any other value of t can also be chosen to highlight this trend.

Condition set	Original value of d	d(0.2)	d(0.4)	d(0.6)	d(0.8)	Time after which two global maxima exist

1	1.3	0.26	0.52	0.78	1.04	0.8
2	2.3	0.46	0.92	1.38	1.84	0.6
3	3.3	0.66	1.32	1.98	2.64	0.4
4	4.3	0.86	1.72	2.58	3.44	0.4
5	5.3	1.06	2.12	3.18	4.24	0.4

Table 4.1.1 - table expressing how the value of time after which two global maxima surely exist in the resultant graph varies with the original value d and d(t).

Note that the value of time after which two global maxima exist is only an approximation because the plots only analysed the following values of t: 0.2, 0.4, 0.6 and 0.8. Actual values may be lesser.

The next characteristic to consider would be the number of peaks per resultant graph (i.e., in each condition set at each time frame). In general, it was hard to suggest a consistent trend for peak count for Gaussian wave packets, because each condition set had a different trend. The following table briefly describes the trend in each condition set.

Condition set	Trend of peak count
1	Constant value of 17, except at t=0.6 at which the peak count was 15.
2	Varied peak count, values ranged from 19 to 27. No similarities and values increased as time progressed, the rate of which was not constant.
3	Varied peak count, values ranged from 25 to 37. No similarities and values increased as time progressed, the rate of which was constant at 4 as time incremented by 0.2.
4	Varied peak count, values ranged from 31 to 47. No similarities and values increased as time progressed, the rate of which was constant at either 4 or 6 as time incremented by 0.2.

5	Varied peak count, values ranged from 39 to 61. No similarities and values increased as time progressed, the rate of which was constant at either 8 or 6 as time incremented by 0.2.

Table 4.1.2 - table expressing how peak count varied as time progressed, for each condition set.

These results, while somewhat erratic, can also be explained using existing literature.

The general and consistent trend of peak count increasing over time is intuitive, as wave packets are further apart with time (d(t) increases), so there is more oscillation space in the centre region and fringes are packed closer together, leading to an increase in peak count.

However, the first condition set does not follow this rule at all, and seemingly contradicts it as the peak count at t [0,0.4] is greater than the peak count at t = 0.6.

We suggest that this result can be explained using the parameters' values in condition set 1. In this set, γ = 0.7, d = 1.3, which means that this condition set has the least separation and the most overlap.

Moreover, when d is small and wave packets are strongly overlapping, interference is broader and smoother. Plus, at t = 0.4, d(t) = 0.52, possibly the transition point where peaks are no longer fully resolved, but not yet narrow enough to produce more detectable maxima.

This could cause the loss of one or two smaller peaks that just fall below the threshold of detectability at that specific distance. This last reason is supported by the functioning of the model which only detects peaks if they are at within 1% of the value of I_max and are also compulsorily at least 10 data points apart in the 2000 data points domain (to only consider natural peaks and avoid counting changes in intensity too small to be considered point of interference). When an interference pattern is clustered due to the parameters' values as in condition set 1, this could cause the model to reject or ignore certain local peaks and only consider the 17-odd 'major' peaks that adhere to both the requirements.

For higher sets, this may also explain why the 'rate of increase of peak count' was not constant.

The Gaussian envelope may also have influenced the number of peaks as it damps the amplitude. As slit separation d increases, the wave packets move further apart. So now the interference happens more in the tails of the Gaussian envelope. The tails are inherently having

very weak amplitudes, which means that fringes that form at the tail of the envelope have very low intensity profiles. Recall that each 'peak' is a point of complete constructive interference, which makes up one 'bright' fringe. Hence, changes in peak count and fringe count are correlated in that manner.

Some of those fringes may become so weak in intensity that they don't show up clearly or don't pass the find_peaks() function's cutoff as explained earlier.

The fourth and the last characteristic to address with regard to time evolution in Gaussian wave packets was the consistency of I_min and I_max values.

The following table briefly describes the effect of the progression of time on I_min and I_max for each condition set.

Condition set	Trend in I_min	Trend in I_max
1	Decreased non-linearly.	Increased and decreased non-linearly.
2	Increased non-linearly till t=0.4 after which it decreased till t=0.6 before increasing till t=0.8.	Decreased non-linearly, before increasing at t=0.6, and then decreases till t=0.8.
3	Value was approximately constant at all points of time.	Value decreased till t=0.6 after which it was approximately constant.
4	Value was approximately constant at all points of time.	Value decreased till t=0.6 after which it was approximately constant.
5	Value was approximately constant at all points of time.	Value decreased till t=0.6 after which it was approximately constant.

Table 4.1.3 - table expressing how the values of I_min and I_max varied as time progressed, for each condition set.

Both trends in I_min and I_max can be explained using existing research as well.

As time progresses, there is more overlap of waves in the central region but greater separation

in general, which causes the bright bands to have a greater intensity and causes the darker bands to have an even lower intensity.

This explains the trend for both I_min and I_max in condition set 1. These results suggest a build up of constructive interference and separation of wave fronts as time progresses, which is consistent with double-slit interference.

For I_min in condition set 2, the oscillation in minimum intensity likely reflects constructive interference at normally dark fringe positions, meaning imperfect destructive interference occurred at that point in time (when the value altered).

However, in condition set 2, the value of I_max exhibited complex behaviour, possibly from the Gaussian damping combined with interference fringes shifting in position. Peaks might be moving out of the observed domain or changing amplitude with wave packet spreading.

For every other condition set, I_min was approximately constant from t=0.2 to t=0.8, which is likely when interference contrast becomes stable. It implies stable destructive interference, meaning coherence is preserved well for higher slit separations or broader overlap regions.

However, the trend for I_max from sets 3 to 5 is of particular interest. The trend shows that the normalised peak intensity initially decreases over time (due to the wave packets spreading), but then stabilises at later time steps. This suggests an 'equilibrium' of sorts between envelope dispersion and fringe narrowing. While this behavior is consistent with quantum interference theory, it is a computationally underexplored phenomenon that may offer insights into time-evolving coherence in wave packet interference.

4.2 interference patterns with Gaussian wave packets

As stated previously, the two observable metrics considered for this study are fringe count and maximum intensity. The following tables summarise the results obtained for these metrics using Gaussian wave packets.

Condition set	Global maximum intensity at time, t			
	t=0.2	t=0.4	t=0.6	t=0.8
1	1.243993	1.463977	1.150208	0.880396
2	1.324242	0.811454	0.916027	0.748049
3	1.150103	0.780206	0.674200	0.679821

4	0.914895	0.728420	0.548617	0.536670
5	0.753760	0.618867	0.480640	0.502405

Table 4.2.1 - table expressing how the values I_max varied for each condition set when using Gaussian wavepackets.

Regardless of which column is taken, there is a steady trend at all points of time for the Global maximum intensity, I_max. The above data shows that as the slit separation, the width of the wave packets and the wave number cumulatively increase, the maximum intensity decreases. An apparent anomaly occurs at t=0.2 as the global maximum intensity for condition set 2 is greater than that for condition set 1 at the same time. We attribute this to the early sampling time combined with the relatively small slit separation in condition set 1. At such short times the two Gaussian packets overlap strongly and the resulting interference pattern is highly sensitive to small changes in phase and position; moreover, envelope damping can suppress or redistribute intensity in a nonmonotonic fashion. Together, these effects can produce transient deviations from the overall decreasing trend in I_max

The observed decline in global maximum intensity I_max with increasing slit separation d, wave packet width γ, and wave number k is consistent with established wave mechanics. As slit separation increases, the angular separation between fringes also increases, causing the central peak to spread over a wider area, thus distributing energy more broadly and reducing peak intensity. A wider wave packet in position space (larger γ) corresponds to a narrower spread in momentum space, but may also induce partial decoherence between contributions from each slit, thereby diminishing the amplitude of constructive interference. Additionally, an increase in wave number k results in shorter wavelengths and more closely spaced fringes, which further diffuses intensity unless the system remains perfectly coherent. These compounded effects explain the systematic decrease in I_max observed in the data. Recall that as the condition set progressed from one to five, the value of the wave number (k) and slit separation (d) increased.

The next observed metric, fringe count in each condition set, is expressed by table 4.2.2.

Condition set	Fringe count			
	t=0.2	t=0.4	t=0.6	t=0.8
1	34	34	30	34
2	38	42	52	54

3	50	58	66	74
4	62	74	82	94
5	78	94	106	122

Table 4.2.2 - table expressing how fringe count varied for each condition set using Gaussian wavepackets.

As shown in Table 4.2.2, the fringe count increases at all time points as we progress from condition set 1 to 5. This behavior is expected as increasing the slit separation, d, reduces the fringe spacing according to the following equation:

$$\Delta x \propto \frac{\lambda}{d} \quad \textbf{(12)}$$

This produces more fringes across the same observation range. Likewise, increasing the wave number k decreases the wavelength, as seen by the following equation:

$$k = \frac{2\pi}{\lambda} \quad \textbf{(13)}$$

$$\Rightarrow \lambda = \frac{2\pi}{k} \quad \textbf{(14)}$$

Which ultimately increases fringe density. These two effects compound, leading to the monotonic increase in fringe count from condition set 1 to 5.

Next, the following sections will now discuss results obtained using Lorentzian wave packets, and any statistical difference that arose from their usage.

4.3 Time evolution with Lorentzian wave packet

The essence of this section will be to compare how time progression influenced characteristics of the resultant graphs in comparison to those arising from the usage of Gaussian wave packets.

Condition set	Original value of d	d(0.2)	d(0.4)	d(0.6)	d(0.8)	Time after which two global maxima exist	Time at which three global maxima exist
1	1.3	0.26	0.52	0.78	1.04	0.4	0.2
2	2.3	0.46	0.92	1.38	1.84	0.4	-
3	3.3	0.66	1.32	1.98	2.64	0.4	-
4	4.3	0.86	1.72	2.58	3.44	0.2	-
5	5.3	1.06	2.12	3.18	4.24	0.2	-

Table 4.3.1 - table expressing how the value of time after which two global maxima surely exist in the resultant graph varies with the original value d and d(t).

Here, we can observe two main differences from the trends observed from the usage of Gaussian wave packets. The first change is how fast two global maxima exist on the plots. Other than in condition set 3 (where the times were the same), all times were lesser when using Lorentzian wave packets. Another notable difference was the presence of three global maxima at t=0.2 in condition set 1. This was not true anywhere else, in any condition set, at any point in time, neither for Lorentzian nor Gaussian wave packets. Both these cases are relatively odd, as Lorentzian wave packets have longer tails (slower decay rate) so the time taken should have been less. Moreover, having 3 distinct peaks is also unexpected behaviour.

When using Lorentzian wave packets, the time at which two global maxima first appear in the interference pattern is generally shorter than for Gaussian wave packets. This makes the consistent trend in table 4.3.1 seem wrong. However, this behaviour can be understood by considering two key features of the Lorentzian envelope. First, despite the presence of long tails, the central peak of a Lorentzian profile can be narrower and more sharply defined than that of a Gaussian. As the two wave packets begin to separate, this sharper central lobe loses its dominance more rapidly, allowing competing maxima to emerge sooner. Second, Lorentzian profiles exhibit a slower decay in amplitude away from the central peak, resulting in relatively stronger side fringes compared to the Gaussian case. These stronger fringes persist further from the origin and can match or exceed the central peak intensity earlier in time as the separation increases.

The combined effect of a rapidly diminishing central maximum and comparatively robust side fringes explains why the onset of two distinct global maxima occurs at an earlier time for Lorentzian wave packets than Gaussian wave packets. We hence theorise that the underlying shape of the envelope is the cause of this error rather than a significant computational error.

The second trend, of having three distinct peaks, was highly anomalous, and hence was first tested to ensure that it wasn't a computational error. After refining the grid, inspecting ψ_total prior to squaring and using the plt.show() to inspect the graph, the following results were obtained.

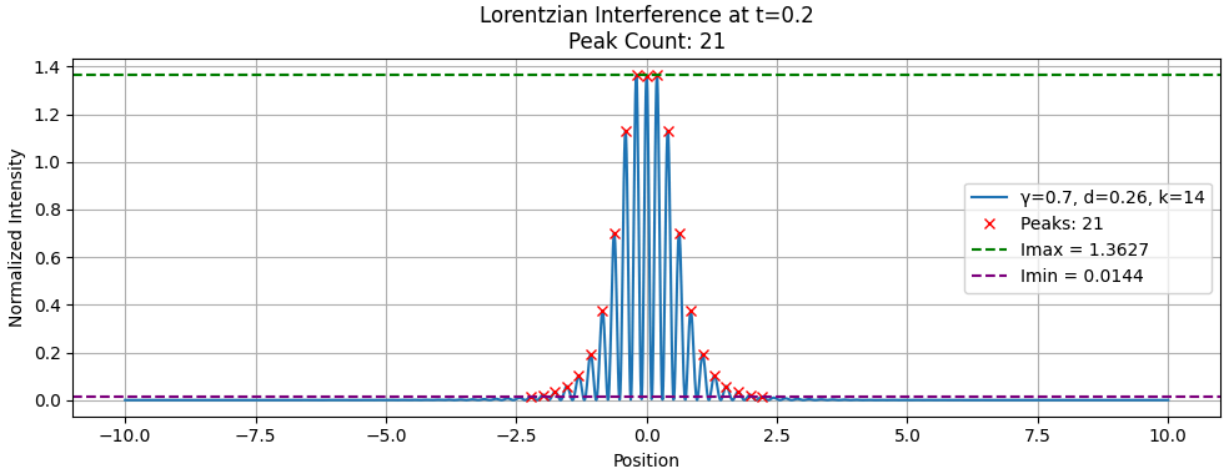

Figure 4.3.1 - graph of normalised intensity against position for condition set 1, time t=0.2. The graph shows three transient peaks.

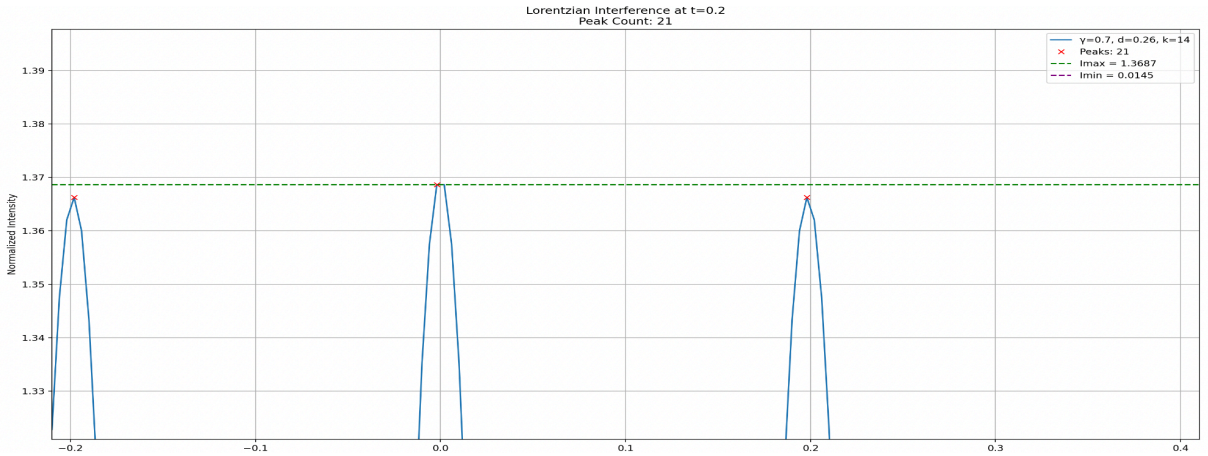

Figure 4.3.2 - zoomed-in graph of normalised intensity against position for condition set 1, time t=0.2. The graph shows one clear peak, and two successive close peaks.

Even though the test revealed that there was only one 'true' global maxima, the values are within 0.05 units of each other, and may even be considered equal by approximation. In any case, this result is still unexpected and requires a novel approach to explain its characteristics.

The occurrence of three near-equal maxima in the central region of the Lorentzian interference pattern can be attributed to the combined effects of the envelope shape and the carrier wave interference. The total field may be expressed as:

$$\Psi_{total}(x) = E_1(x)cos(k[x - x_1]) + E_2(x)cos(k[x - x_2]) \quad \textbf{(15)}$$

where E1,2(x) are the Lorentzian envelopes centered at x1,2=±d(t)/2. In this formulation, the fast interference fringes, with a spatial period of approximately 2π/k, are modulated by a slower envelope governed by the factor cos(kd/2). When cos(kd/2) is not large, the amplitude of the central fringe can be comparable to that of its adjacent fringes. This effect is not observed for the Gaussian profile with the same d and k parameters in the same condition set, due to its more rapid high-frequency attenuation, which significantly reduces the relative amplitude of the adjacent peaks.

Lorentzian envelopes have heavy tails, which enhance the relative strength of side maxima compared to the Gaussian case (i.e. energy doesn't concentrate evenly in one global maximum). Furthermore, the relative carrier phase between the two wave packets, given by kd/2, can approach values that partially suppress the central carrier amplitude. In such cases,

energy is ‘redistributed’ to the neighbouring fringes, producing multiple central maxima of similar height. When the envelopes at positions such as −0.2, 0, and +0.2 retain similar magnitudes due to the Lorentzian tail structure, and the local carrier phases in those regions favour constructive interference, the resulting intensity profile naturally exhibits three peaks of comparable amplitude in the central region.

It is important to note that certain considerations have been made when using this approach to resolve the anomalous result of having three global maxima. The mathematical form of the cos(kd/2) factor is not analytically derived for the simulation and assumes constant k throughout the envelope and assumes that the wave packets are symmetric. It is also only true if the wave packets interlap reasonably enough at the point, but since it was the centre, it was a valid assumption to make. The underlying note is that this is not a formally derived inference, but rather uses existing literature to back the results generated by the model.

The next trend to analyse with regard to time evolution is the trend in peak count. The table summarises these trends.

Condition set	Trend of peak count
1	Constant value of 21, except at t=0.2 at which the peak count was 23.
2	Peak count constant till t=0.6, where it increased from 27 to 28. By t=0.8, this value increased to 33.
3	Varied peak count, values ranged from 35 to 47. No similarities and values increased as time progressed, the rate of which was not constant.
4	Varied peak count, values ranged from 31 to 47. No similarities and values increased as time progressed, the rate of which was constant at either 4 or 6 as time incremented by 0.2.
5	Varied peak count, values ranged from 39 to 61. No similarities and values increased as time progressed, the rate of which was constant at either 8 or 6 as time incremented

	by 0.2.

Table 4.3.2 - table expressing how peak count varied as time progressed, for each condition set, now using Lorentzian wave packets.

Analysing these trends, we can point out two pertinent features when comparing results from Lorentzian and Gaussian wavepackets: one, the results for condition sets 4 and 5 are identical, regardless of the wave packet used. Two, condition sets 1 through 3 we see that the values of peak count are higher when using Lorentzian rather than Gaussian wave packets, however the range of values is lesser from t=0.2 to t=0.8.

Characteristic one suggests that after reaching a certain value in γ, d and k, the effect of the shape of the wave packet is negligible. This means that the interference pattern produced is more due to the geometric composition of the setup than the wave packet. This judgement is also evidenced by the fact that there was variation in condition sets 1 through 3, where the values of γ,d and k were comparatively smaller.

The second characteristic was to be expected as well. Lorentzian wave packets have longer, heavier tails and have ‘bursts’ of energy expressed as higher values in peak count (i.e. greater intensity peaks, but they are more concentrated around the centre). Gaussian wave packets spread more over time, hence there are more peaks overall, even though the value of those peaks may be lower.

The last trend to address with regard to time evolution in Lorentzian wave packets was the consistency of I_min and I_max values.

The following table briefly describes the effect of the progression of time on I_min and I_max for each condition set.

Condition set	Trend in I_min	Trend in I_max
1	Decreased till t=0.4, then increased, both at nonlinear rates.	Increased till t=0.4, then decreased, both at nonlinear rates.
2	Increased non-linearly till t=0.6, after which it decreased till t=0.8	Increased and decreased non-linearly, alternatively from t=0.2 to t=0.8.
3	Value was approximately	Value decreased till t=0.6

	constant at all points in time.	after which it was approximately constant.
4	Value was approximately constant at all points in time.	Value decreased till t=0.6 after which it was approximately constant.
5	Value was approximately constant at all points in time.	Value decreased till t=0.6 after which it was approximately constant.

Table 4.3.3 - table expressing how the values of I_min and I_max varied as time progressed, for each condition set, now using Lorentzian wave packets.

A clear contrast emerged between the time-evolution of fringe intensities for Gaussian and Lorentzian wavepackets, particularly in Condition Sets 1 and 2. For Lorentzian packets, both I_min and I_max) exhibited pronounced nonlinear reversals—such as a decrease followed by recovery, or alternating increases and decreases—reflecting the inherently unstable evolution of heavy-tailed waveforms. These behaviors arise from the Lorentzian's broad momentum distribution and long spatial tails, which cause rapid early-time decoherence across the slits and generate strong temporal beating between widely separated frequency components.

By contrast, Gaussian packets produced much smoother and more monotonic trends: I_min typically decayed gradually as coherence decreased, while I_max showed gentle variations without the sharp oscillations characteristic of Lorentzian profiles. This difference indicates that Gaussian packets retain temporal coherence more reliably, whereas Lorentzian packets undergo repeated coherence loss and partial revival. Condition Set 2 emphasized this divergence even more strongly; Lorentzian I_max oscillated throughout the evolution interval, while the Gaussian counterpart varied predictably and without abrupt contrast reversals. Overall, the discrepancies demonstrate that interference from non-Gaussian, heavy-tailed wavepackets is far more sensitive to dispersion and phase-mixing effects, leading to a richer but less stable temporal structure in the interference pattern.

Observe that the trend for I_max from sets 3 to 5 is sustained even for Lorentzian wavepackets, which further reinforces the claim that there is an equilibrium that is reached between envelope dispersion and fringe narrowing, potentially making it independent of the wavepacket form used, as this occurred at the same sets for both wavepacket forms.

4.4 interference patterns with Lorentzian wave packets

The following tables summarise the results obtained for fringe counts and maximum intensities, now using Lorenwave packets.

Condition set	Global maximum intensity at time, t			
	t=0.2	t=0.4	t=0.6	t=0.8
1	1.362668	1.460705	1.088957	1.034853
2	1.383771	0.956111	1.043856	0.859163
3	1.149877	0.768712	0.777455	0.816795
4	0.888404	0.847302	0.630627	0.587326
5	0.744345	0.717406	0.549876	0.552125

Table 4.4.1 - table expressing how the values I_max varied for each condition set when using Lorentzian wavepackets.

As indicated above, the general trend of the peak intensity decreasing as the wave number, slight separation and wavelength increased was also present when using Lorentzian wavepackets as the wave's angular separation will increase with slit separation, regardless of the wavepacket used, continuing to decrease the peak intensity as examined previously. Coincidentally, the 'apparent anomaly' at t=0.2 was also present here, presumably for the same reason, attributed to the early sampling time combined with the relatively small slit separation in condition set 1, leading to some amount of potential dampening that reduced the global maximum intensity.

Thus, although the early-time maxima for Gaussian and Lorentzian wavepackets are comparable, the Lorentzian profiles consistently produce lower maximum intensities as time progresses. This trend is especially pronounced in Condition Sets 3 to 5, where the Gaussian peaks remain higher at all time points. The result is consistent with the heavier-tailed Lorentzian packets dispersing more rapidly, whilst the Gaussian wavepackets are 'concentrated' towards the centre with lighter tails,leading to reduced constructive interference contrast compared to the Gaussian case.

Lastly, the next table (table 4.4.2) describes the variance of fringe counts for each condition set.

Condition set	Fringe count			
	t=0.2	t=0.4	t=0.6	t=0.8
1	42	46	46	46
2	58	58	56	66
3	70	74	78	86
4	86	88	102	114
5	102	106	126	142

Table 4.4.2 - table expressing how fringe count varied for each condition set using Lorentzian wavepackets.

As can be deduced from table 4.4.2, there are two clear distinctions in fringe count variance arising from the use of different wavepackets.

The first difference is that the Lorentzian wavepackets generated a greater fringe count than Gaussian wavepackets in the double-slit interference pattern. This expectation follows from the fundamental differences in how the two wavepacket types distribute their energy.

A Lorentzian packet possesses heavy spatial tails and a much broader momentum spectrum, decaying as $1/k^2$ rather than the rapid Gaussian fall-off of $\exp(-k^2)$. As a result, the Lorentzian contains a larger population of high-momentum components, which translates into smaller fringe spacing and therefore a higher density of fringes. Furthermore, Lorentzian packets undergo faster and more extensive dispersion during time evolution: their heavy tails contribute amplitude far from the packet centre, allowing the overall interference envelope to spread more rapidly. This wider envelope accommodates a larger number of fringes, especially at later times, whereas the Gaussian's quickly vanishing tails confine the region over which visible interference can occur. Taken together, the combination of enhanced dispersion, extended spatial support, and richer high-frequency content leads us to predict that Lorentzian wavepackets should consistently exhibit a greater fringe count than their Gaussian counterparts.

(5) Conclusion

Across all simulations, Gaussian and Lorentzian wavepackets displayed clear and systematic differences in how they evolve and form double-slit interference patterns. Gaussian packets transitioned from a single central maximum to two dominant peaks with time, with larger slit separations producing this transition earlier and yielding more fringes overall; however, strong early overlap caused some nonlinear behaviour and suppressed minor peaks.

Lorentzian packets, with their heavy tails, evolved faster; secondary maxima became competitive earlier, fringe amplitudes persisted farther out, and an unusual three-peak structure emerged under specific low-distance conditions, which was concluded to be a characteristic (slower rate of attenuation) of the Lorentzian wavepacket since this effect was not observed when using Gaussian wavepackets.

In both envelopes, increasing slit separation and wave number consistently increased fringe counts and reduced peak intensities, but Lorentzians always produced more fringes due to their broader momentum distribution. Despite these differences, both packet types eventually reached similar qualitative intensity trends at large separations, indicating that geometry dominates long-time behaviour. Overall, the results show that wavepacket shape strongly influences early-time interference features, while the large-scale structure is controlled primarily by slit geometry and wavelength.

(6) Acknowledgements

The author thanks Ms. Manik Higne for their support and guidance in determining the applications of the results in current scientific contexts.

(7) References

[1]Greenberger, Daniel M, et al. *Compendium of Quantum Physics : Concepts, Experiments, History, and Philosophy*. Heidelberg ; New York, Springer, 2009, pp. 828–830.

[2]Heisenberg, Werner. "Über den anschaulichen Inhalt der quantentheoretischen Kinematik und Mechanik." *Zeitschrift für Physik* 43.3 (1927): 172-198.

[3] Fitzpatrick, Richard. *Quantum Mechanics*. World Scientific Publishing Company, 19 May 2015.

[4]Oda, Kin-ya, and Juntaro Wada. “Lorentz-Covariant Spinor Wave Packet.” *Physical Review. D/Physical Review. D.*, vol. 110, no. 7, 1 Oct. 2024, https://doi.org/10.1103/physrevd.110.076001. Accessed 13 Dec. 2025.

[5] Dieks, Dennis & Nienhuis, Gerard. (1990). Relativistic aspects of nonrelativistic quantum mechanics. American Journal of Physics - AMER J PHYS. 58. 650-655. 10.1119/1.16426.

[6]Baiguera, Stefano. "Aspects of Non-Relativistic Quantum Field Theories." *Arxiv.org*, 2024, arxiv.org/html/2311.00027v2. Accessed 13 Dec. 2025.

[7]Pavšič, M. Localized States in Quantum Field Theory. *Adv. Appl. Clifford Algebras* 28, 89 (2018). https://doi.org/10.1007/s00006-018-0904-5

[8] Hung-Ming Tsai and Bill Poirier 2016 *J. Phys.: Conf. Ser.* **701** 012013

[9] Padmanabhan, T.. (2018). Obtaining the non-relativistic quantum mechanics from quantum field theory: issues, folklores and facts: What happens to the antiparticles when you take the non-relativistic limit of QFT?. The European Physical Journal C. 78. 10.1140/epjc/s10052-018-6039-y.

[10] Baldo, Marcello. (2025). Lorentz Transformation in Quantum Mechanics. 10.48550/arXiv.2511.11342.

[11] Makris, Nicos, and Gary F. Dargush. "A Real-Valued Description of Quantum Mechanics with Schrödinger's 4th-Order Matter-Wave Equation." *Physics Open*, vol. 23, 14 Mar. 2025, p. 100262,www.sciencedirect.com/science/article/pii/S2666032625000122,https://doi.org/10.1016/j.physo.2025.100262.

[12] Fitzpatrick, Richard. "Normalization of the Wavefunction." *Farside.ph.utexas.edu*, 20 July 2010, farside.ph.utexas.edu/teaching/qmech/Quantum/node34.html.

[13] Read, Dr. Mark S. D. "QM Normalising a Wave Function 3 | Chemistry Outreach." *Chemreach.science*, 2019, chemreach.science/qm-normalising-a-wave-function-3/.

[14] Benyong Chen, Jianbo Luo, and Dacheng Li, "Code counting of optical fringes: methodology and realization," Appl. Opt. **44**, 217-223 (2005)

[15] Gamdan Optics. "Interferometry - Fringes and Phases." *Gamdan Optics*, 3 Nov. 2021, www.gamdan.com/blog/interferometry-fringes-and-phases.

[16] SATHEE . "SATHEE: Physics Youngs Double Slit Experiment." *Iitk.ac.in*, 2025, sathee.iitk.ac.in/article/physics/physics-youngs-double-slit-experiment/.

[17] قسم الفيزياء, et al. المستنصرية الجامعة - العلوم كلية *Lecture (3) Coherence, Thin Film and Fresnel Biprism Edited By*. 2023

[18] Albert, M, and P. Devillard. "Waiting Time Distribution for Trains of Quantized Electron Pulses." *Physical Review B*, vol. 90, no. 3, 22 July 2014, https://doi.org/10.1103/physrevb.90.035431.

[19] Libretexts (Physics). "5.10: Fringe Visibility." *Physics LibreTexts*, 11 Jan. 2022, phys.libretexts.org/Bookshelves/Optics/BSc_Optics_(Konijnenberg_Adam_and_Urbach)/05%3A_Interference_and_coherence/5.10%3A_Fringe_Visibility.

[20] OpenStax. "4.4: Double-Slit Diffraction." *Physics LibreTexts*, 1 Nov. 2016, phys.libretexts.org/Bookshelves/University_Physics/University_Physics_(OpenStax)/University_Physics_III_-_Optics_and_Modern_Physics_(OpenStax)/04%3A_Diffraction/4.04%3A_Double-Slit_Diffraction.

[21] Kok, Pieter, and Brendon W Lovett. *Introduction to Optical Quantum Information Processing*. Cambridge University Press, 22 Apr. 2010, p. 27.

[22] Koch, Dr. Erik. "Gaussian Wave Packets." *Cond-Mat.de*, 2025, www.cond-mat.de/teaching/QM/JSim/wpack.html.

[23] Hanson, David M., et al. "3.6: Wavefunctions Must Be Normalized." *Chemistry LibreTexts*, 17 June 2014, chem.libretexts.org/Bookshelves/Physical_and_Theoretical_Chemistry_Textbook_Maps/Physical_Chemistry_(LibreTexts)/03%3A_The_Schrodinger_Equation_and_a_Particle_in_a_Box/3.06%3A_Wavefunctions_Must_Be_Normalized.

[24] GeeksforGeeks. "Trapezoidal Rule." *GeeksforGeeks*, 21 June 2021, www.geeksforgeeks.org/maths/trapezoidal-rule/.

[25] Božić, Mirjana & Davidović, Milena & Dimitrova, Todorka & Miret-Artés, Salvador & Sanz, Angel & Weis, Antoine. (2010). Generalized Arago-Fresnel laws: The EME-flow-line description. Journal of Russian Laser Research. 31. 117-128. 10.1007/s10946-010-9131-9.

.